

## Extracting the Pomeron-Pomeron- $f_2(1270)$ coupling in the $pp \rightarrow pp\pi^+\pi^-$ reaction through the angular distribution of the pions

Piotr Lebedowicz<sup>1,\*</sup>, Otto Nachtmann<sup>2,†</sup> and Antoni Szczurek<sup>1,‡,§</sup>

<sup>1</sup>*Institute of Nuclear Physics Polish Academy of Sciences, Radzikowskiego 152, PL-31342 Kraków, Poland*

<sup>2</sup>*Institut für Theoretische Physik, Universität Heidelberg, Philosophenweg 16, D-69120 Heidelberg, Germany*

 (Received 14 December 2019; accepted 16 January 2020; published 11 February 2020)

We discuss how to extract the Pomeron-Pomeron- $f_2(1270)$  [ $\mathbb{P}\mathbb{P}f_2(1270)$ ] coupling within the tensor-Pomeron model. The general  $\mathbb{P}\mathbb{P}f_2(1270)$  coupling is a combination of seven basic couplings (tensorial structures). To study these tensorial structures, we propose to measure the central-exclusive production of a  $\pi^+\pi^-$  pair in the invariant mass region of the  $f_2(1270)$  meson. An analysis of angular distributions in the  $\pi^+\pi^-$  rest system, using the Collins-Soper and the Gottfried-Jackson frames, turns out to be particularly relevant for our purpose. For both frames, the  $\cos\theta_{\pi^+}$  and  $\phi_{\pi^+}$  distributions are discussed. We find that the azimuthal angle distributions in these frames are fairly sensitive to the choice of the  $\mathbb{P}\mathbb{P}f_2$  coupling. We show results for the resonance case alone as well as when the dipion continuum is included. We show the influence of the experimental cuts on the angular distributions in the context of dedicated experimental studies at RHIC and LHC energies. Absorption corrections are included for our final distributions.

DOI: 10.1103/PhysRevD.101.034008

### I. INTRODUCTION

The Pomeron ( $\mathbb{P}$ ) is an essential object for understanding diffractive phenomena in high-energy physics. Within QCD, the Pomeron is a color-singlet, predominantly gluonic object. The spin structure of the Pomeron, and in particular its coupling to hadrons, is, however, not yet a matter of consensus. In the tensor-Pomeron model for soft high-energy scattering formulated in Ref. [1], the Pomeron exchange is effectively treated as the exchange of a rank-2 symmetric tensor. The diffractive amplitude for a given process with soft Pomeron exchange can then be formulated in terms of effective propagators and vertices respecting the rules of quantum field theory.

It is rather difficult to obtain definitive statements on the spin structure of the Pomeron from unpolarized elastic proton-proton scattering. On the other hand, the results from polarized proton-proton scattering by the STAR

Collaboration [2] provide valuable information on this question. Three hypotheses for the spin structure of the Pomeron, tensor, vector, and scalar were discussed in Ref. [3] in view of the experimental results from Ref. [2]. Only the tensor ansatz for the Pomeron was found to be compatible with the experiment. Also, some historical remarks on different views of the Pomeron were made in Ref. [3].

In Ref. [4], further strong evidence against the hypothesis of a vector character of the Pomeron was given. It was shown there that a vector Pomeron necessarily decouples in elastic photon-proton scattering and in the absorption cross sections of virtual photons on the proton—that is, in the structure functions of deep inelastic lepton-nucleon scattering. A tensor Pomeron, on the other hand, has no such problems, and tensor-Pomeron exchanges, soft and hard, give an excellent description of the absorption cross sections for real and virtual photons on the proton at high energies.

In the last few years we have undertaken a scientific program to analyze the production of light mesons in the tensor-Pomeron and vector-Odderon approach in several exclusive reactions:  $pp \rightarrow ppM$  [5],  $pp \rightarrow pp\pi^+\pi^-$  [6,7],  $pp \rightarrow pn\rho^0\pi^+$  ( $pp\rho^0\pi^0$ ) [8],  $pp \rightarrow ppK^+K^-$  [9],  $pp \rightarrow pp(\sigma, \rho^0\rho^0 \rightarrow \pi^+\pi^-\pi^+\pi^-)$  [10],  $pp \rightarrow ppp\bar{p}$  [11],  $pp \rightarrow pp(\phi\phi \rightarrow K^+K^-K^+K^-)$  [12], and  $pp \rightarrow pp(\phi \rightarrow K^+K^-, \mu^+\mu^-)$  [13]. Some azimuthal angle correlations between the outgoing protons can verify the  $\mathbb{P}\mathbb{P}M$

\*Piotr.Lebedowicz@ifj.edu.pl

†O.Nachtmann@thphys.uni-heidelberg.de

‡Antoni.Szczurek@ifj.edu.pl

§Also at College of Natural Sciences, Institute of Physics, University of Rzeszów, Pignonia 1, PL-35310 Rzeszów, Poland.

Published by the American Physical Society under the terms of the [Creative Commons Attribution 4.0 International license](https://creativecommons.org/licenses/by/4.0/). Further distribution of this work must maintain attribution to the author(s) and the published article's title, journal citation, and DOI. Funded by SCOAP<sup>3</sup>.

couplings for scalar  $f_0(980)$ ,  $f_0(1370)$ ,  $f_0(1500)$ ,  $f_0(1710)$  and pseudoscalar  $\eta$ ,  $\eta'(958)$  mesons [5,9]. The couplings, being of nonperturbative nature, are difficult to obtain from first principles of QCD. The corresponding coupling constants were fitted to differential distributions of the WA102 Collaboration [14–16] and to the results of Ref. [17]. As was shown in Ref. [5,9], the tensorial  $\mathbb{P}\mathbb{P}f_0$ ,  $\mathbb{P}\mathbb{P}\eta$ , and  $\mathbb{P}\mathbb{P}\eta'$  vertices correspond to the sum of the two lowest orbital angular momentum–spin couplings, except for the  $f_0(1370)$  meson. The tensor meson case is a bit complicated, as there are, in our approach, seven possible Pomeron-Pomeron- $f_2(1270)$  couplings in principle; see the list of possible  $\mathbb{P}\mathbb{P}f_2$  couplings in Appendix A of Ref. [7] and in Sec. II below.

It was shown in Refs. [15,18] that the cross section for the undisputed  $q\bar{q}$  tensor mesons,  $f_2(1270)$  and  $f_2'(1525)$ , peaks at  $\phi_{pp} = \pi$  and is suppressed at small  $dP_t$  in contrast to the tensor glueball candidate  $f_2(1950)$ ; see, e.g., Ref. [19]. Here,  $\phi_{pp}$  is the azimuthal angle between the transverse momentum vectors  $\mathbf{p}_{t,1}$  and  $\mathbf{p}_{t,2}$  of the outgoing protons, and  $dP_t$  (the so-called “glueball filter variable” [20]) is defined by their difference  $d\mathbf{P}_t = \mathbf{p}_{t,2} - \mathbf{p}_{t,1}$ ,  $dP_t = |d\mathbf{P}_t|$ . In Ref. [7], we gave some arguments from studying the  $\phi_{pp}$  and  $dP_t$  distributions that one particular coupling  $\mathbb{P}\mathbb{P}f_2$  (denoted by  $j = 2$ ) may be preferred. We roughly reproduced the experimental data obtained by the WA102 Collaboration [15] and by the ABCDHW Collaboration [21] with this coupling. It was demonstrated in Ref. [7] that the relative contribution of the resonant  $f_2(1270)$  and dipion continuum strongly depends on the cut on four-momentum transfer squared  $t_{1,2}$  in a given experiment. However, we must remember that at low energies, the secondary (especially  $f_{2\mathbb{R}}$  Reggeon) exchanges may also play an important role.

Now, we ask the question of whether and how the  $\mathbb{P}\mathbb{P}f_2$  couplings can be studied in central-exclusive processes. In the present work, we discuss such a possibility: the analysis of angular distributions of pions from the decay of  $f_2$ , in two systems of reference, the Collins-Soper (CS) and the Gottfried-Jackson (GJ) systems. We will consider diffractive production of the  $f_2(1270)$  resonance, which is expected to be abundantly produced in the  $pp \rightarrow pp\pi^+\pi^-$  reaction; see, e.g., Ref. [7]. We will try to analyze whether

such a study could shed light on the  $\mathbb{P}\mathbb{P}f_2(1270)$  couplings. In Refs. [22–24], the central-exclusive production of two-pseudoscalar mesons in  $pp$  collisions at the COMPASS experiment at CERN SPS was reported. There, preliminary data of pion angular distributions in the  $\pi^+\pi^-$  rest system using the GJ frame was shown. We refer the reader to Refs. [25–30] for the latest measurements of central  $\pi^+\pi^-$  production in high-energy proton-(anti)proton collisions. In the future, the corresponding  $\mathbb{P}\mathbb{P}f_2(1270)$  couplings could be adjusted by comparison to precise experimental data from both the RHIC and the LHC.

## II. FORMALISM

We study the central-exclusive production of  $\pi^+\pi^-$  in proton-proton collisions:

$$p(p_a, \lambda_a) + p(p_b, \lambda_b) \rightarrow p(p_1, \lambda_1) + \pi^+(p_3) + \pi^-(p_4) + p(p_2, \lambda_2), \quad (2.1)$$

where  $p_{a,b}$ ,  $p_{1,2}$  and  $\lambda_{a,b}$ ,  $\lambda_{1,2} \in \{+1/2, -1/2\}$  denote the four-momenta and helicities of the protons, and  $p_{3,4}$  denote the four-momenta of the charged pions, respectively.

We are, in the present article, mainly interested in the region of the  $\pi^+\pi^-$  invariant mass in the  $f_2(1270)$  region. There we should take into account two main processes shown by the diagrams in Fig. 1. For the  $f_2(1270)$  resonance [Fig. 1(a)], we consider only the  $\mathbb{P}\mathbb{P}$  fusion. The secondary Reggeons  $f_{2\mathbb{R}}$ ,  $a_{2\mathbb{R}}$ ,  $\omega_{\mathbb{R}}$ ,  $\rho_{\mathbb{R}}$  should give small contributions at high energies. We also neglect contributions involving the photon. In the case of the nonresonant continuum [Fig. 1(b)], we include in the calculations both  $\mathbb{P}$  and  $f_{2\mathbb{R}}$ -Reggeon exchanges. For an extensive discussion, we refer to Refs. [6,7].

The kinematic variables for the reaction in Eq. (2.1) are

$$\begin{aligned} s &= (p_a + p_b)^2, & s_{34} &= M_{\pi\pi}^2 = (p_3 + p_4)^2, \\ q_1 &= p_a - p_1, & q_2 &= p_b - p_2, & t_1 &= q_1^2, & t_2 &= q_2^2, \\ p_{34} &= q_1 + q_2 = p_3 + p_4, \\ s_1 &= (p_a + q_2)^2 = (p_1 + p_{34})^2, \\ s_2 &= (p_b + q_1)^2 = (p_2 + p_{34})^2. \end{aligned} \quad (2.2)$$

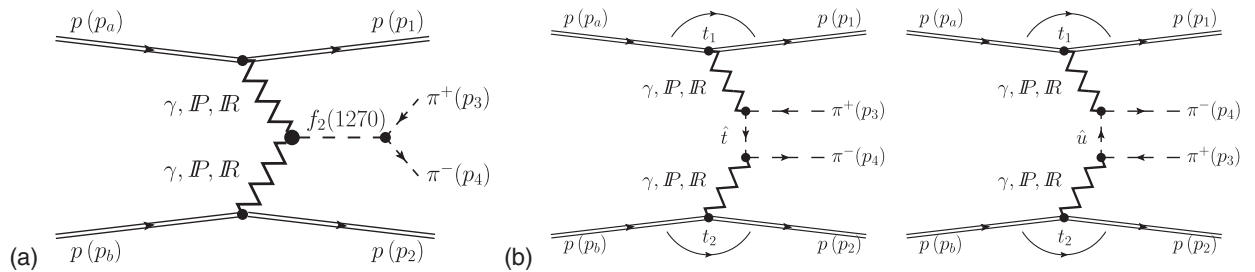


FIG. 1. The Born diagrams for the  $pp \rightarrow pp\pi^+\pi^-$  reaction. In (a), we have the  $\pi^+\pi^-$  production via the  $f_2(1270)$  resonance; in (b), the continuum  $\pi^+\pi^-$  production. The exchange objects are the photon ( $\gamma$ ), the Pomeron ( $\mathbb{P}$ ), and the Reggeons ( $\mathbb{R}$ ).

The  $\mathbb{P}\mathbb{P}$ -exchange (Born-level) amplitude for  $\pi^+\pi^-$  production via the tensor  $f_2$ -meson [ $f_2 \equiv f_2(1270)$ ] exchange can be written as

$$\begin{aligned} \mathcal{M}_{\lambda_a \lambda_b \rightarrow \lambda_1 \lambda_2 \pi^+ \pi^-}^{(\mathbb{P}\mathbb{P} \rightarrow f_2 \rightarrow \pi^+ \pi^-)} &= (-i) \bar{u}(p_1, \lambda_1) i \Gamma_{\mu_1 \nu_1}^{(\mathbb{P}\mathbb{P})} (p_1, p_a) u(p_a, \lambda_a) i \Delta^{(\mathbb{P}) \mu_1 \nu_1, \alpha_1 \beta_1} (s_1, t_1) \\ &\times i \Gamma_{\alpha_1 \beta_1, \alpha_2 \beta_2, \rho \sigma}^{(\mathbb{P}\mathbb{P} f_2)} (q_1, q_2) i \Delta^{(f_2) \rho \sigma, \alpha \beta} (p_{34}) i \Gamma_{\alpha \beta}^{(f_2 \pi \pi)} (p_3, p_4) \\ &\times i \Delta^{(\mathbb{P}) \alpha_2 \beta_2, \mu_2 \nu_2} (s_2, t_2) \bar{u}(p_2, \lambda_2) i \Gamma_{\mu_2 \nu_2}^{(\mathbb{P}\mathbb{P})} (p_2, p_b) u(p_b, \lambda_b). \end{aligned} \quad (2.3)$$

Here  $\Delta^{(\mathbb{P})}$  and  $\Gamma^{(\mathbb{P}\mathbb{P})}$  denote the effective propagator and proton vertex functions, respectively, for the tensor-Pomeron exchange. For the explicit expressions, see Sec. III of Ref. [1]. More details related to the amplitude [Eq. (2.3)] are given in Ref. [7].  $\Delta^{(f_2)}$  and  $\Gamma^{(f_2 \pi \pi)}$  denote the tensor-meson propagator and the  $f_2 \pi \pi$  vertex, respectively. As was mentioned in Ref. [1], we cannot use a simple Breit-Wigner ansatz for the  $f_2$  propagator in conjunction with the  $f_2 \pi \pi$  vertex from Eqs. (3.37) and (3.38) of Ref. [1], because the partial-wave unitarity relation is not satisfied. We should use, therefore, a model for the  $f_2$  propagator considered in Eqs. (3.6)–(3.8) and (5.19)–(5.22) of Ref. [1]. The form factor  $F^{(f_2 \pi \pi)}(p_{34}^2)$  for the  $f_2 \pi \pi$  vertex and for the  $f_2$  propagator is taken to be the same as in Eq. (2.7) below, but with  $\Lambda_{f_2 \pi \pi}$  instead of  $\Lambda_{\mathbb{P}\mathbb{P} f_2}$ .

The main ingredient of the amplitude [Eq. (2.3)] is the Pomeron-Pomeron- $f_2$  vertex<sup>1</sup>

$$i \Gamma_{\mu\nu, \kappa\lambda, \rho\sigma}^{(\mathbb{P}\mathbb{P} f_2)} (q_1, q_2) = \left( i \Gamma_{\mu\nu, \kappa\lambda, \rho\sigma}^{(\mathbb{P}\mathbb{P} f_2)(1)} |_{\text{bare}} + \sum_{j=2}^7 i \Gamma_{\mu\nu, \kappa\lambda, \rho\sigma}^{(\mathbb{P}\mathbb{P} f_2)(j)} (q_1, q_2) |_{\text{bare}} \right) \tilde{F}^{(\mathbb{P}\mathbb{P} f_2)} (q_1^2, q_2^2, p_{34}^2). \quad (2.4)$$

Here  $\tilde{F}^{(\mathbb{P}\mathbb{P} f_2)}$  is a form factor for which we make a factorized ansatz [see Eq. (4.17) of Ref. [7]]:

$$\tilde{F}^{(\mathbb{P}\mathbb{P} f_2)} (q_1^2, q_2^2, p_{34}^2) = F_M(q_1^2) F_M(q_2^2) F^{(\mathbb{P}\mathbb{P} f_2)} (p_{34}^2). \quad (2.5)$$

We are taking here the same form factor for each vertex with index  $j$  ( $j = 1, \dots, 7$ ). In principle, we could take a different form factor for each vertex. We take

$$F_M(t) = \frac{1}{1 - t/\Lambda_0^2}, \quad \Lambda_0^2 = 0.5 \text{ GeV}^2; \quad (2.6)$$

$$F^{(\mathbb{P}\mathbb{P} f_2)} (p_{34}^2) = \exp\left(\frac{-(p_{34}^2 - m_{f_2}^2)^2}{\Lambda_{\mathbb{P}\mathbb{P} f_2}^4}\right), \quad \Lambda_{\mathbb{P}\mathbb{P} f_2} = 1 \text{ GeV}. \quad (2.7)$$

The expressions for our bare vertices in Eq. (2.4), obtained from the coupling Lagrangians in Appendix A of Ref. [7], are as follows:

$$i \Gamma_{\mu\nu, \kappa\lambda, \rho\sigma}^{(\mathbb{P}\mathbb{P} f_2)(1)} = 2i g_{\mathbb{P}\mathbb{P} f_2}^{(1)} M_0 R_{\mu\nu\mu_1\nu_1} R_{\kappa\lambda\alpha_1\lambda_1} R_{\rho\sigma\rho_1\sigma_1} g^{\nu_1\alpha_1} g^{\lambda_1\rho_1} g^{\sigma_1\mu_1}, \quad (2.8)$$

$$i \Gamma_{\mu\nu, \kappa\lambda, \rho\sigma}^{(\mathbb{P}\mathbb{P} f_2)(2)} (q_1, q_2) = -\frac{2i}{M_0} g_{\mathbb{P}\mathbb{P} f_2}^{(2)} ((q_1 \cdot q_2) R_{\mu\nu\rho_1\alpha} R_{\kappa\lambda\sigma_1}{}^\alpha - q_{1\rho_1} q_2^{\mu_1} R_{\mu\nu\mu_1\alpha} R_{\kappa\lambda\sigma_1}{}^\alpha - q_1^{\mu_1} q_{2\sigma_1} R_{\mu\nu\rho_1\alpha} R_{\kappa\lambda\mu_1}{}^\alpha + q_{1\rho_1} q_{2\sigma_1} R_{\mu\nu\kappa\lambda}) R_{\rho\sigma}{}^{\rho_1\sigma_1}, \quad (2.9)$$

$$i \Gamma_{\mu\nu, \kappa\lambda, \rho\sigma}^{(\mathbb{P}\mathbb{P} f_2)(3)} (q_1, q_2) = -\frac{2i}{M_0} g_{\mathbb{P}\mathbb{P} f_2}^{(3)} ((q_1 \cdot q_2) R_{\mu\nu\rho_1\alpha} R_{\kappa\lambda\sigma_1}{}^\alpha + q_{1\rho_1} q_2^{\mu_1} R_{\mu\nu\mu_1\alpha} R_{\kappa\lambda\sigma_1}{}^\alpha + q_1^{\mu_1} q_{2\sigma_1} R_{\mu\nu\rho_1\alpha} R_{\kappa\lambda\mu_1}{}^\alpha + q_{1\rho_1} q_{2\sigma_1} R_{\mu\nu\kappa\lambda}) R_{\rho\sigma}{}^{\rho_1\sigma_1}, \quad (2.10)$$

$$i \Gamma_{\mu\nu, \kappa\lambda, \rho\sigma}^{(\mathbb{P}\mathbb{P} f_2)(4)} (q_1, q_2) = -\frac{i}{M_0} g_{\mathbb{P}\mathbb{P} f_2}^{(4)} (q_1^{\alpha_1} q_2^{\mu_1} R_{\mu\nu\mu_1\nu_1} R_{\kappa\lambda\alpha_1\lambda_1} + q_2^{\alpha_1} q_1^{\mu_1} R_{\mu\nu\alpha_1\lambda_1} R_{\kappa\lambda\mu_1\nu_1}) R^{\nu_1\lambda_1}{}_{\rho\sigma}, \quad (2.11)$$

<sup>1</sup>Here the label ‘‘bare’’ is used for a vertex, as derived from a corresponding coupling Lagrangian in Appendix A of Ref. [7] without a form-factor function; see Eqs. (2.8)–(2.14) below.

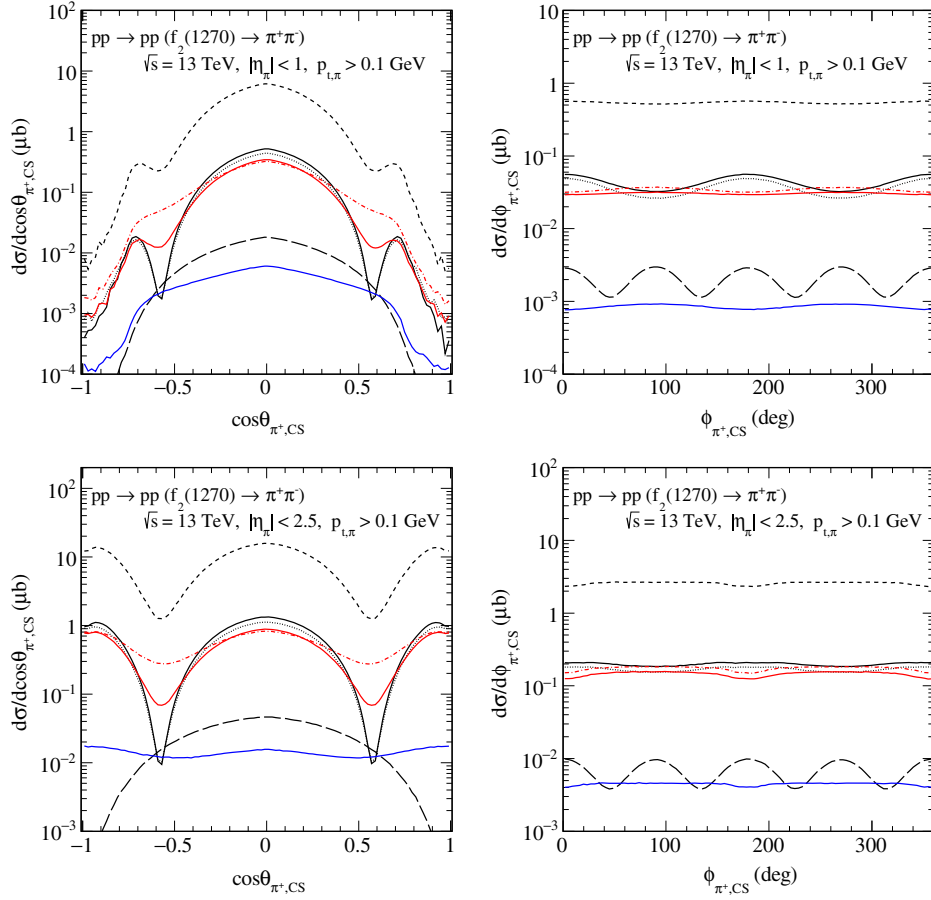


FIG. 2. The distributions in  $\cos\theta_{\pi^+,CS}$  (the left panels) and in  $\phi_{\pi^+,CS}$  (the right panels) for the  $pp \rightarrow pp[f_2(1270) \rightarrow \pi^+\pi^-]$  reaction. The calculations were performed for  $\sqrt{s} = 13$  TeV with different cuts on  $|\eta_\pi|$  and  $p_{t,\pi} > 0.1$  GeV. The individual contributions of the different  $\mathbb{P}\mathbb{P}f_2$  couplings from Eqs. (2.8) to (2.14) are shown:  $j = 1$  (the black solid line),  $j = 2$  (the black long-dashed line),  $j = 3$  (the black dashed line),  $j = 4$  (the black dotted line),  $j = 5$  (the blue solid line),  $j = 6$  (the red solid line), and  $j = 7$  (the red dot-dashed line). The results correspond to the arbitrary choice of coupling constants  $g_{\mathbb{P}\mathbb{P}f_2}^{(j)} = 1.0$ . No absorption effects were included here.

$$i\Gamma_{\mu\nu,\kappa\lambda,\rho\sigma}^{(\mathbb{P}\mathbb{P}f_2)^{(5)}}(q_1, q_2) = -\frac{2i}{M_0^3} g_{\mathbb{P}\mathbb{P}f_2}^{(5)} (q_1^\mu q_2^\nu R_{\mu\nu\alpha} R_{\kappa\lambda\mu}{}^\alpha + q_1^\nu q_2^\mu R_{\mu\nu\alpha} R_{\kappa\lambda\nu}{}^\alpha - 2(q_1 \cdot q_2) R_{\mu\nu\kappa\lambda}) q_{1\alpha_1} q_{2\lambda_1} R^{\alpha_1\lambda_1}{}_{\rho\sigma}, \quad (2.12)$$

$$i\Gamma_{\mu\nu,\kappa\lambda,\rho\sigma}^{(\mathbb{P}\mathbb{P}f_2)^{(6)}}(q_1, q_2) = \frac{i}{M_0^3} g_{\mathbb{P}\mathbb{P}f_2}^{(6)} (q_1^\alpha q_1^{\lambda_1} q_2^\mu q_{2\rho_1} R_{\mu\nu\mu_1\nu_1} R_{\kappa\lambda\alpha_1\lambda_1} + q_2^\alpha q_2^{\lambda_1} q_1^\mu q_{1\rho_1} R_{\mu\nu\alpha_1\lambda_1} R_{\kappa\lambda\mu_1\nu_1}) R^{\nu_1\rho_1}{}_{\rho\sigma}, \quad (2.13)$$

$$i\Gamma_{\mu\nu,\kappa\lambda,\rho\sigma}^{(\mathbb{P}\mathbb{P}f_2)^{(7)}}(q_1, q_2) = -\frac{2i}{M_0^3} g_{\mathbb{P}\mathbb{P}f_2}^{(7)} q_1^{\rho_1} q_1^{\alpha_1} q_1^{\lambda_1} q_2^{\sigma_1} q_2^\mu q_2^{\nu_1} R_{\mu\nu\mu_1\nu_1} R_{\kappa\lambda\alpha_1\lambda_1} R_{\rho\sigma\rho_1\sigma_1}, \quad (2.14)$$

where

$$R_{\mu\nu\kappa\lambda} = \frac{1}{2} g_{\mu\kappa} g_{\nu\lambda} + \frac{1}{2} g_{\mu\lambda} g_{\nu\kappa} - \frac{1}{4} g_{\mu\nu} g_{\kappa\lambda}. \quad (2.15)$$

In Eqs. (2.8) to (2.14), the Lorentz indices of the Pomeron with four-momentum  $q_1$  are denoted by  $\mu\nu$ , those of the Pomeron with four-momentum  $q_2$  by  $\kappa\lambda$ , and those of the  $f_2$

by  $\rho\sigma$ . Furthermore,  $M_0 \equiv 1$  GeV, and then  $g_{\mathbb{P}\mathbb{P}f_2}^{(j)}$  ( $j = 1, \dots, 7$ ) are dimensionless coupling constants. The values of the coupling constants  $g_{\mathbb{P}\mathbb{P}f_2}^{(j)}$  are not known and are not easy to be found from first principles of QCD, as they are of nonperturbative origin. At the present stage, these coupling constants  $g_{\mathbb{P}\mathbb{P}f_2}^{(j)}$  should be fitted to experimental data.

Considering the fictitious reaction of two “real tensor Pomerons” annihilating to the  $f_2$  meson (see Appendix A

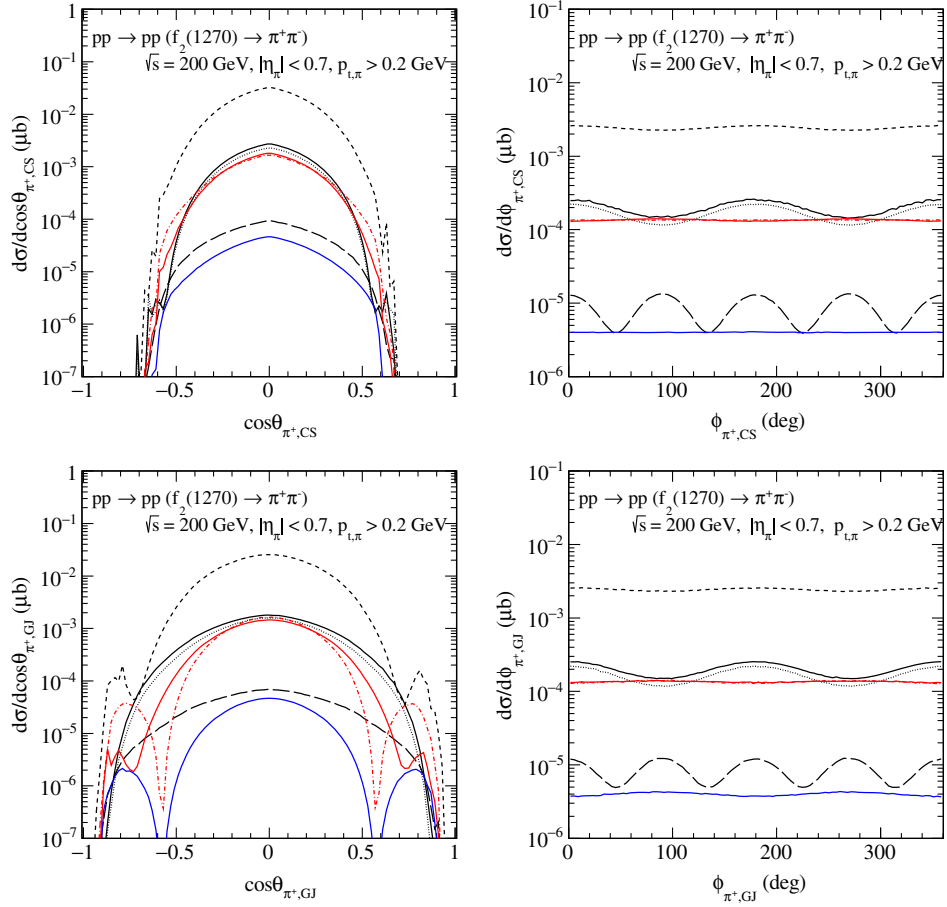


FIG. 3. The same as in Fig. 2, but for  $\sqrt{s} = 200$  GeV and the STAR experimental cuts from Ref. [28]:  $|\eta_\pi| < 0.7$ ,  $p_{T,\pi} > 0.2$  GeV, and with cuts on the leading protons [Eq. (3.1)]. In the top panels, we show the pion angular distributions in the  $\pi^+\pi^-$  rest system using the CS frame [Eq. (2.16)]. In the bottom panels, we show the results using the GJ frame [Eq. (2.18)].

of Ref. [7]), we find that we can associate the couplings in Eqs. (2.8)–(2.14) with the following  $(l, S)$  values<sup>2</sup>:  $(0, 2)$ ,  $(2, 0) - (2, 2)$ ,  $(2, 0) + (2, 2)$ ,  $(2, 4)$ ,  $(4, 2)$ ,  $(4, 4)$ , and  $(6, 4)$ , respectively.

To give the full physical amplitudes, we should include absorptive corrections to the Born amplitudes. For the details on how to include the  $pp$ -rescattering corrections in the eikonal approximation for the four-body reaction, see, e.g., Sec. 3.3 of Ref. [6]. Other rescattering corrections, such as possible pion-proton [31,32] and pion-pion [33] interactions in the final state, and also so-called “enhanced” corrections [34], are neglected in the present calculations. In practice, we work with the amplitudes in the high-energy approximation; see Eqs. (3.19)–(3.21) and (4.23) of Ref. [7].

We are interested in the angular distribution of the  $\pi^+$  in the center-of-mass system of the  $\pi^+\pi^-$  pair. Various reference systems are commonly used; see, e.g., Ref. [35] for a discussion of such systems for the

$\gamma p \rightarrow \pi^+\pi^-p$  reaction. For the Collins-Soper system [36,37] for the reaction in Eq. (2.1), we set the unit vectors defining the axes as follows:

$$\begin{aligned} \mathbf{e}_{3,\text{CS}} &= \frac{\hat{\mathbf{p}}_a - \hat{\mathbf{p}}_b}{|\hat{\mathbf{p}}_a - \hat{\mathbf{p}}_b|}, \\ \mathbf{e}_{2,\text{CS}} &= \frac{\hat{\mathbf{p}}_a \times \hat{\mathbf{p}}_b}{|\hat{\mathbf{p}}_a \times \hat{\mathbf{p}}_b|}, \\ \mathbf{e}_{1,\text{CS}} &= \frac{\hat{\mathbf{p}}_a + \hat{\mathbf{p}}_b}{|\hat{\mathbf{p}}_a + \hat{\mathbf{p}}_b|}. \end{aligned} \quad (2.16)$$

These satisfy the condition  $\mathbf{e}_{1,\text{CS}} = \mathbf{e}_{2,\text{CS}} \times \mathbf{e}_{3,\text{CS}}$ . Here  $\hat{\mathbf{p}}_a = \mathbf{p}_a/|\mathbf{p}_a|$ ,  $\hat{\mathbf{p}}_b = \mathbf{p}_b/|\mathbf{p}_b|$ , where  $\mathbf{p}_a$ ,  $\mathbf{p}_b$  are the three-momenta of the initial protons in the  $\pi^+\pi^-$  rest system. There we have  $\mathbf{p}_{34} = 0$  and  $\mathbf{p}_a + \mathbf{p}_b = \mathbf{p}_1 + \mathbf{p}_2$ . Now we denote by  $\theta_{\pi^+,\text{CS}}$  and  $\phi_{\pi^+,\text{CS}}$  the polar and azimuthal angles of  $\hat{\mathbf{p}}_3$  (the  $\pi^+$  meson momentum) relative to the coordinate axes [Eq. (2.16)]. We have then, e.g.,

$$\cos \theta_{\pi^+,\text{CS}} = \hat{\mathbf{p}}_3 \cdot \mathbf{e}_{3,\text{CS}}, \quad (2.17)$$

where  $\hat{\mathbf{p}}_3 = \mathbf{p}_3/|\mathbf{p}_3|$ .

<sup>2</sup>Here,  $l$  and  $S$  denote the orbital angular momentum and total spin of two fictitious “real Pomerons” in the rest system of the  $f_2$  meson, respectively.

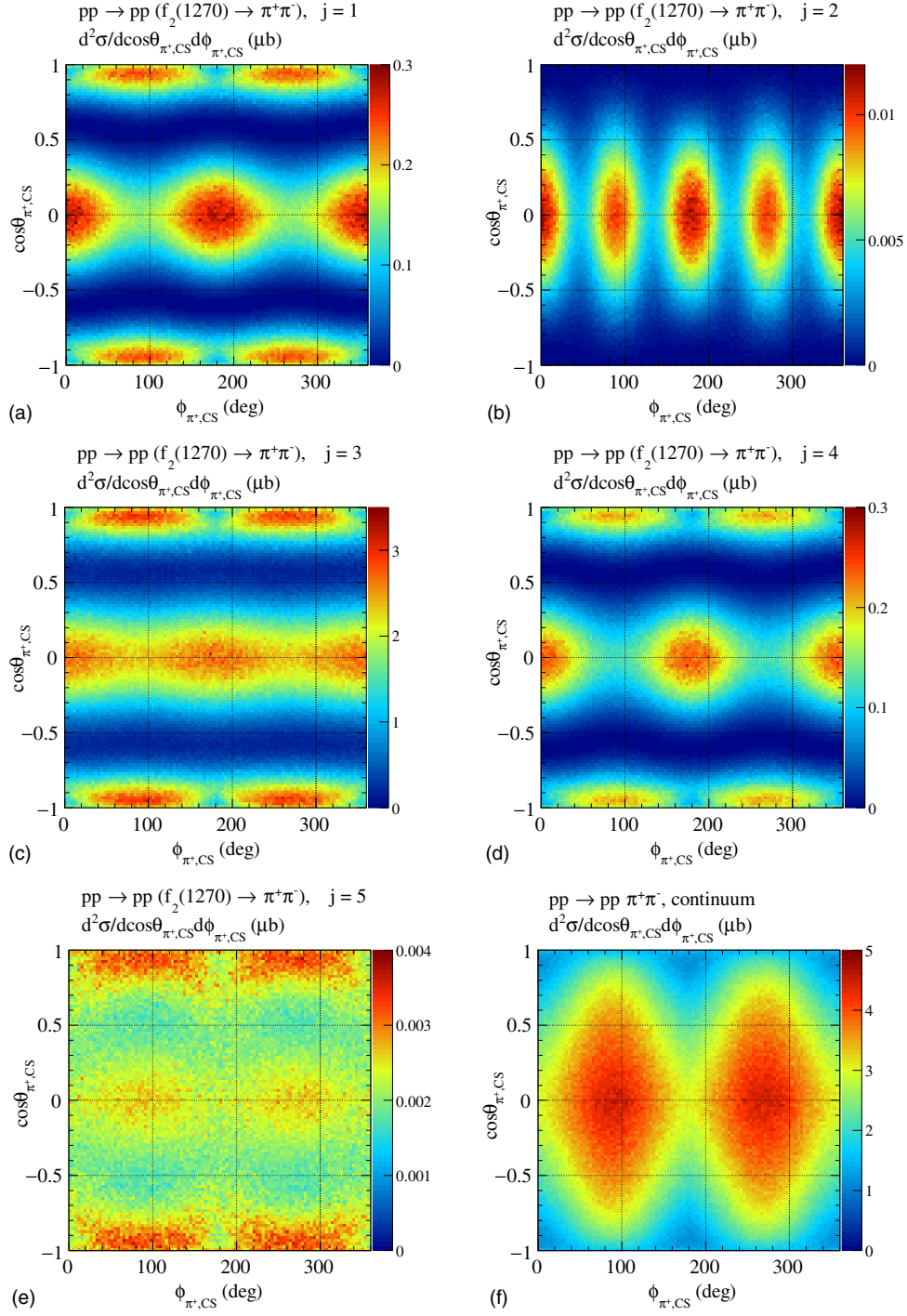


FIG. 4. The two-dimensional distributions in  $(\phi_{\pi^+,CS}, \cos\theta_{\pi^+,CS})$  for the  $pp \rightarrow pp\pi^+\pi^-$  reaction. The calculations were done for  $\sqrt{s} = 13$  TeV and with cuts on  $|\eta_\pi| < 2.5$ . The individual  $f_2(1270) \rightarrow \pi^+\pi^-$  contributions for five  $\mathbb{P}\mathbb{P}f_2$  couplings, (a)  $j = 1$ , (b)  $j = 2$ , (c)  $j = 3$ , (d)  $j = 4$ , (e)  $j = 5$ , and (f) the  $\pi^+\pi^-$  continuum term are presented. The results for  $\pi^+\pi^-$  production via  $f_2(1270)$  resonance were obtained with coupling constants  $g_{\mathbb{P}\mathbb{P}f_2}^{(j)} = 1.0$ . No absorption effects were included here.

Alternatively, for the experiments that can measure at least one of the outgoing protons, the Gottfried-Jackson (GJ) system could be used as well. For the GJ system [38], we set

$$\mathbf{e}_{3,GJ} = \frac{\mathbf{q}_1}{|\mathbf{q}_1|}, \quad \mathbf{e}_{2,GJ} = \frac{\mathbf{q}_{1,c.m.} \times \mathbf{q}_{2,c.m.}}{|\mathbf{q}_{1,c.m.} \times \mathbf{q}_{2,c.m.}|}, \quad \mathbf{e}_{1,GJ} = \mathbf{e}_{2,GJ} \times \mathbf{e}_{3,GJ}. \quad (2.18)$$

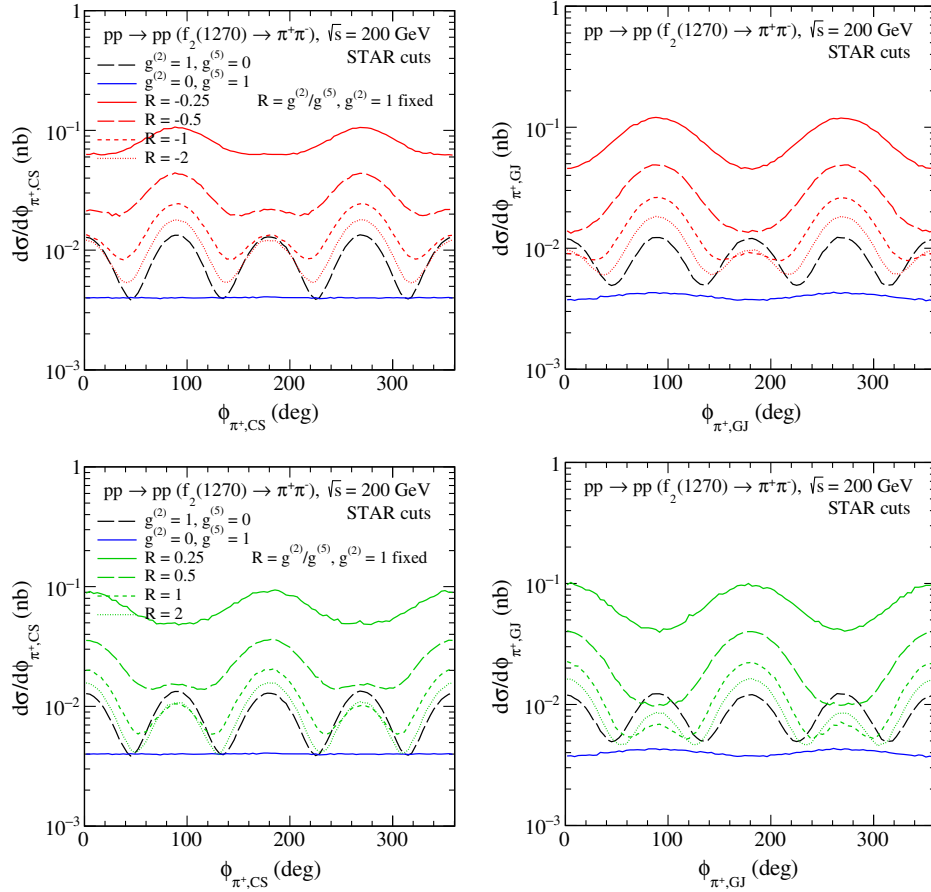


FIG. 5. The distributions in azimuthal angle in the  $\pi^+\pi^-$  rest system using the CS frame (left panels) and the GJ frame (right panels). The calculations were done for the STAR kinematics (see the caption of Fig. 3). No absorption effects were included here.

Here  $\mathbf{q}_1$  is the three-momentum of the Pomeron (emitted by the proton with positive  $p_z$ ) in the  $\pi^+\pi^-$  rest system. The second axis of the GJ coordinate system is fixed by the normal to the production plane ( $\mathbb{P}\text{-}\mathbb{P}\text{-}\pi^+\pi^-$  plane) in the  $pp$  center-of-mass (c.m.) system.  $\mathbf{q}_{1,\text{c.m.}}$  and  $\mathbf{q}_{2,\text{c.m.}}$  are three-momenta defined in the  $pp$  c.m. frame.

For some further remarks on this GJ system, see the Appendix.

Having defined these angles, we can now examine the differential cross sections  $d^2\sigma/(d\cos\theta_{\pi^+,\text{CS}}d\phi_{\pi^+,\text{CS}})$ ,  $d\sigma/d\cos\theta_{\pi^+,\text{CS}}$ ,  $d\sigma/d\phi_{\pi^+,\text{CS}}$ , and the corresponding distributions in the GJ system.

### III. RESULTS

As discussed in the Introduction, very good observables which can be used for visualizing the role of the  $\mathbb{P}\mathbb{P}f_2$  couplings, given by Eqs. (2.8)–(2.14) (cf. also Appendix A of Ref. [7]), could be the differential cross sections  $d\sigma/d\cos\theta_{\pi^+}$  and  $d\sigma/d\phi_{\pi^+}$ , both in the CS and the GJ systems of reference; see Eqs. (2.16) and (2.18), respectively. In Figs. 2–5 and 7–10, we show such angular distributions for the  $\pi^+$  meson in the  $\pi^+\pi^-$  rest frame.

In Fig. 2, we collect angular distributions for all (seven) independent  $\mathbb{P}\mathbb{P}f_2(1270)$  couplings for  $\sqrt{s} = 13$  TeV,  $p_{t,\pi} > 0.1$  GeV and for two different cuts on the pseudorapidities of the pions,  $|\eta_\pi| < 1.0$  (the top panels) and  $|\eta_\pi| < 2.5$  (the bottom panels), that will be measured in the LHC experiments. In Fig. 3, we show results for the STAR experimental conditions with extra cuts on the leading protons, specified in Ref. [28]:

$$\begin{aligned} (p_{x,p} + 0.3 \text{ GeV})^2 + p_{y,p}^2 &< 0.25 \text{ GeV}^2, \\ 0.2 \text{ GeV} < |p_{y,p}| < 0.4 \text{ GeV}, & \quad p_{x,p} > -0.2 \text{ GeV}. \end{aligned} \quad (3.1)$$

Quite different distributions are obtained for different couplings. Note that the shape of the angular distributions depends on the coverage in  $|\eta_\pi|$ . From the top-left panel in Fig. 2, we see that the condition  $|\eta_\pi| < 1.0$  leads to a reduction of the cross sections mostly at  $\cos\theta_{\pi^+,\text{CS}} \approx \pm 1$  compared to the results with  $|\eta_\pi| < 2.5$  shown in the bottom-left panel. To our surprise, the distributions in azimuthal angle are particularly interesting. The distributions for the resonance contribution alone can be approximated as

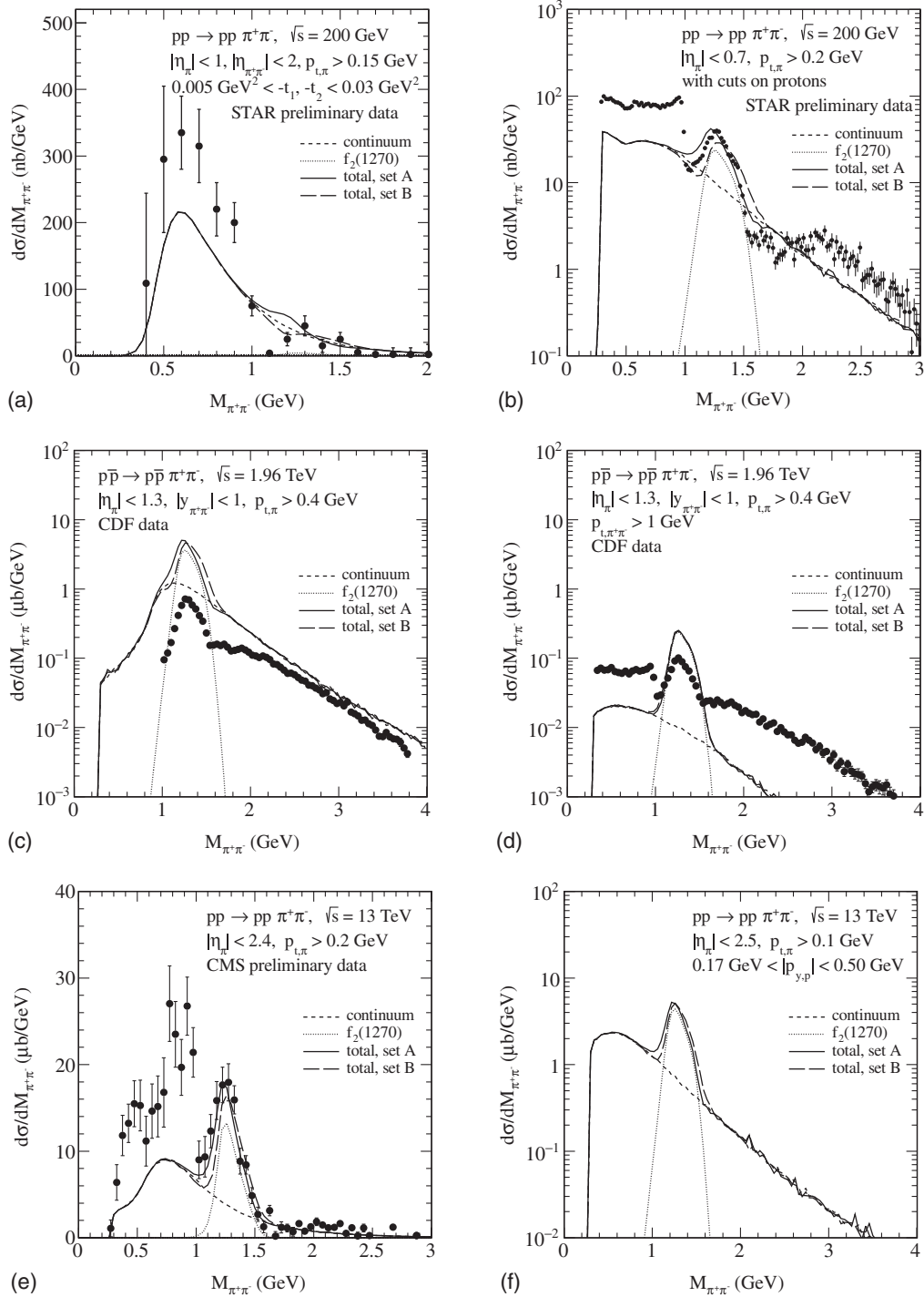


FIG. 6. Two-pion invariant mass distributions with the relevant kinematical cuts for (a),(b) STAR; (c),(d) CDF; (e) CMS; and (f) ATLAS-ALFA experiments. The STAR preliminary data from Refs. [25,28], the CDF data from Ref. [26], and the CMS preliminary data from Ref. [29] are shown. The calculations for the STAR and ATLAS-ALFA experiments were done with extra cuts on the leading protons. The short-dashed lines represent the nonresonant continuum contribution, and the dotted lines represent the results for the  $f_2(1270)$  contribution, while the solid and long-dashed lines represent their coherent sum for the two parameter sets A and B, respectively. Here we take, in set A  $(g_{pp}^{(2)} f_2, g_{pp}^{(5)} f_2) = (-4.0, 16.0)$ , and in set B  $(g_{pp}^{(2)} f_2, g_{pp}^{(5)} f_2) = (4.0, -16.0)$ ; see Eqs. (2.5), (2.9), and (2.12). The absorption effects are included here.

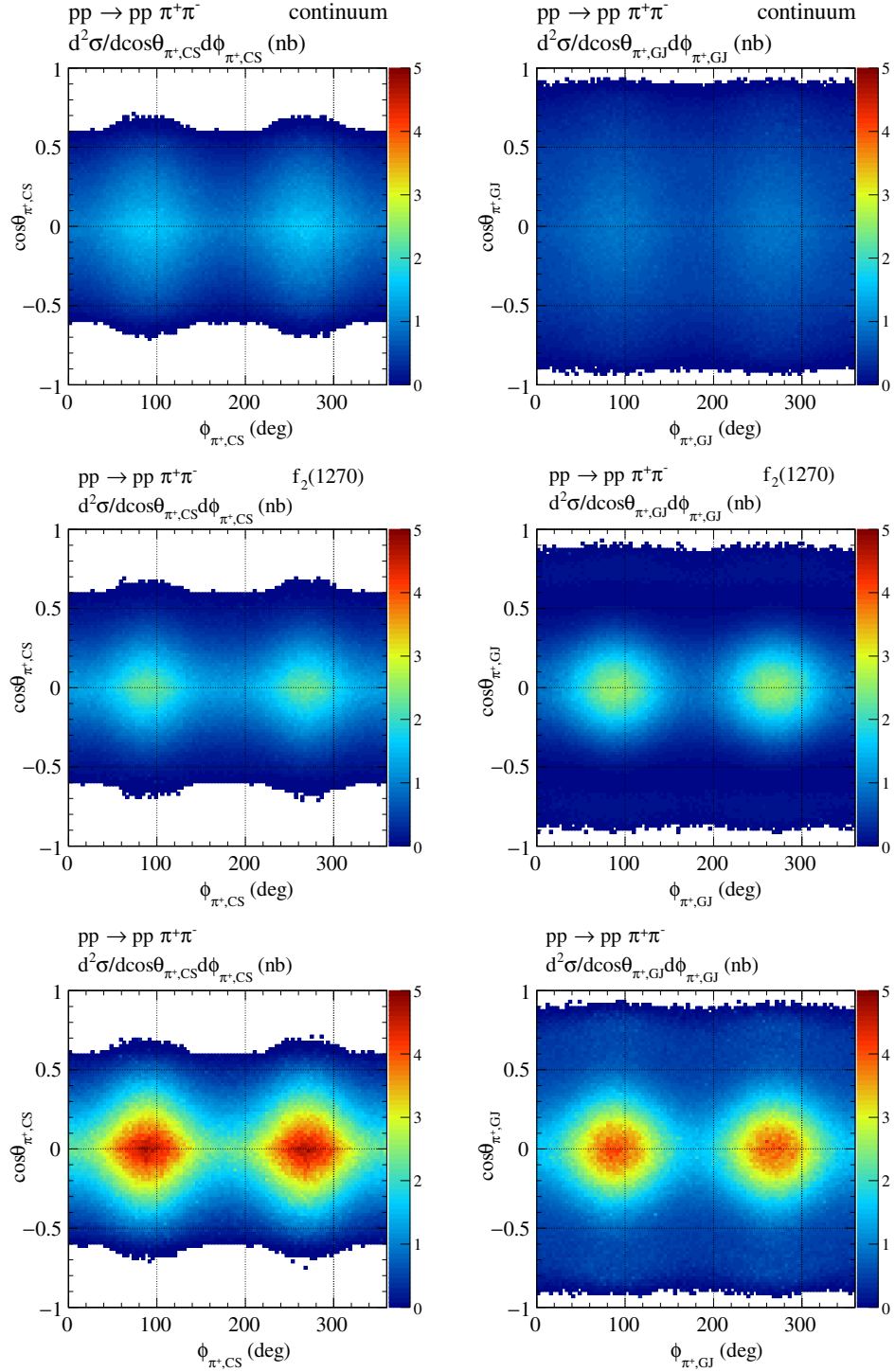


FIG. 7. The distributions in  $(\phi_{\pi^+,CS}, \cos \theta_{\pi^+,CS})$  (the left panels) and in  $(\phi_{\pi^+,GJ}, \cos \theta_{\pi^+,GJ})$  (the right panels) for the  $pp \rightarrow pp\pi^+\pi^-$  reaction. The calculations were done in the dipion invariant mass region  $M_{\pi^+\pi^-} \in (1.0, 1.5)$  GeV for  $\sqrt{s} = 200$  GeV and the STAR experimental cuts from Ref. [28]:  $|\eta_\pi| < 0.7$ ,  $p_{t,\pi} > 0.15$  GeV, and Eq. (3.1). In the top panels, we show results for the  $\pi^+\pi^-$  continuum term; in the center panels, results for the  $f_2(1270)$  resonance term (set A); and in the bottom panels, those for both the contributions added coherently. Here we take  $(g_{\mathbb{P}\mathbb{P}f_2}^{(2)}, g_{\mathbb{P}\mathbb{P}f_2}^{(5)}) = (-4.0, 16.0)$  as discussed in the main text. The absorption effects are included here.

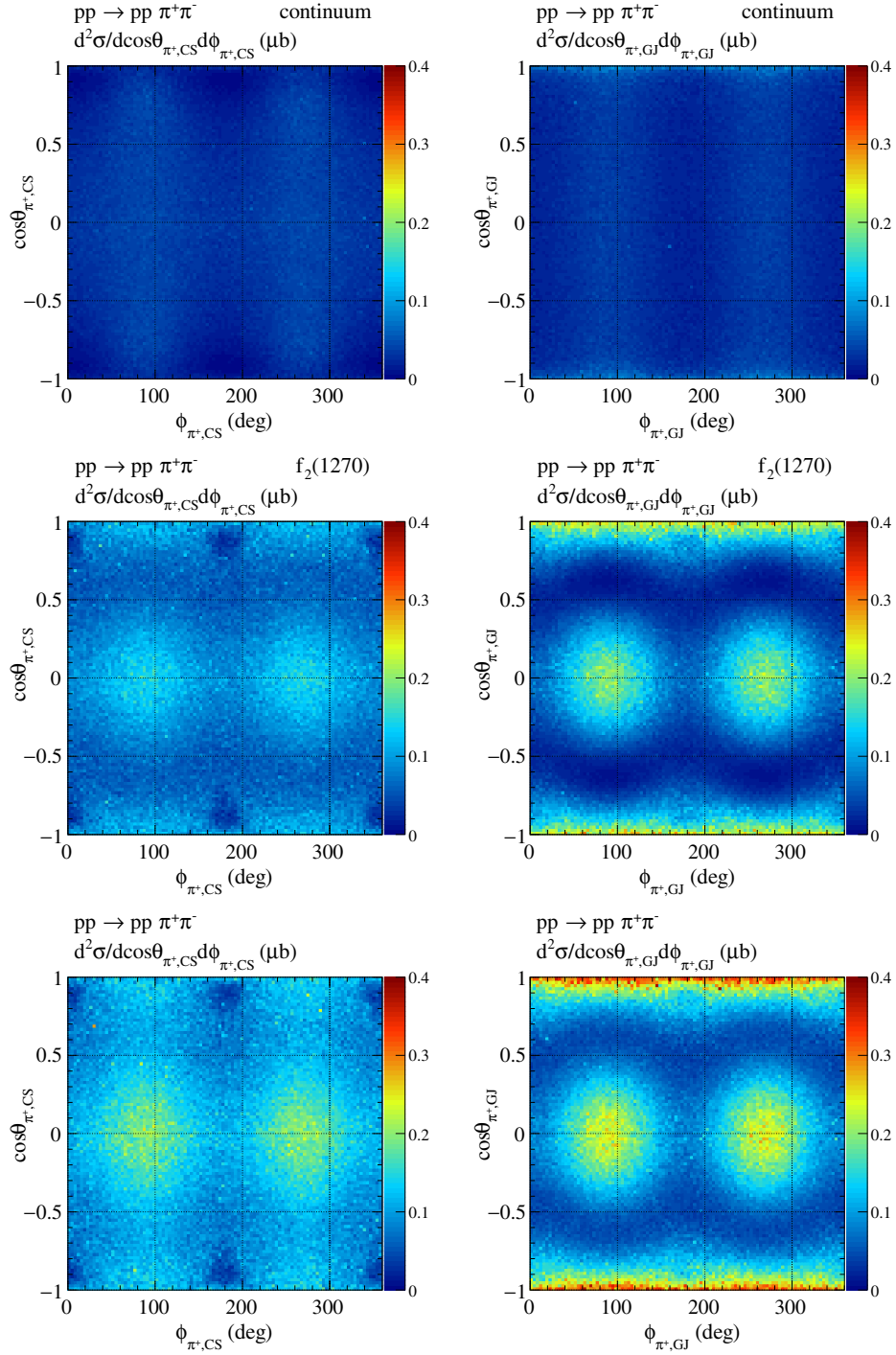


FIG. 8. The same as in Fig. 7, but for  $\sqrt{s} = 13$  TeV and the ATLAS-ALFA experimental cuts:  $|\eta_\pi| < 2.5$ ,  $p_{t,\pi} > 0.1$  GeV, and  $0.17$  GeV  $< |p_{y,p}| < 0.50$  GeV. The calculations were done in the dipion invariant mass region  $M_{\pi^+\pi^-} \in (1.0, 1.5)$  GeV. The absorption effects are included here.

$$d\sigma/d\phi_{\pi^+,CS} \approx A \pm B \cos(n\phi_{\pi^+,CS}) \quad (3.2)$$

for  $|\cos\theta_{\pi^+,CS}| < 0.5$  (as will be shown below), where  $A$  and  $B$  depend on experimental conditions. For most of the couplings  $n = 2$ , but for the  $j = 2$  coupling it is  $n = 4$ . The reader is asked to note the different number of

oscillations for the  $j = 2$  coupling. The shape of  $\phi_{\pi^+,CS}$  distributions depends also on the cuts on  $|\eta_\pi|$ . Therefore, we expect these differences to be better visible when one compares the results related to different regions of pion pseudorapidity. Let us note that the LHCb Collaboration can measure  $\pi^+\pi^-$  production for  $2.0 < \eta_\pi < 4.5$  [39].

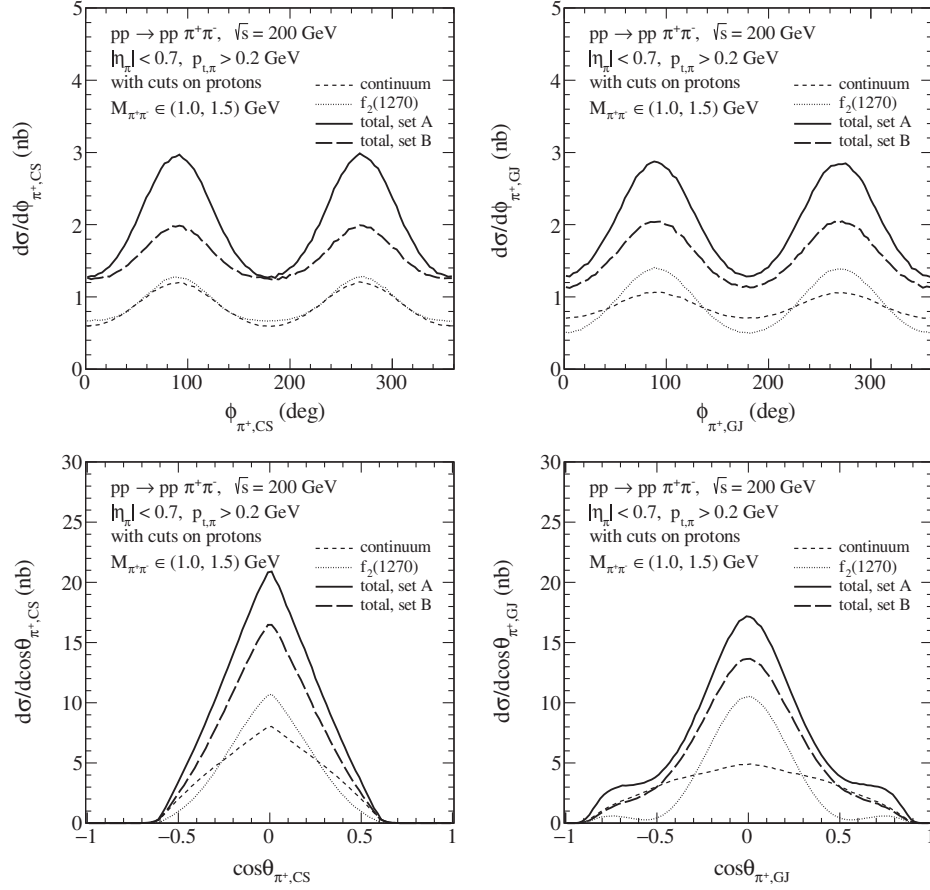


FIG. 9. The angular distributions for the  $pp \rightarrow pp\pi^+\pi^-$  reaction. The calculations were done for  $\sqrt{s} = 200$  GeV in the dipion invariant mass region  $M_{\pi^+\pi^-} \in (1.0, 1.5)$  GeV and for the STAR experimental cuts specified in Ref. [28]. The results for the  $\pi^+\pi^-$  continuum term (the short-dashed line), for the  $f_2(1270)$  resonance term (the dotted line), and for their coherent sum (the solid and long-dashed lines corresponding to sets A and B, respectively) are presented. We have taken here A  $(g_{\mathbb{P}\mathbb{P}f_2}^{(2)}, g_{\mathbb{P}\mathbb{P}f_2}^{(5)}) = (-4.0, 16.0)$ , and B  $(g_{\mathbb{P}\mathbb{P}f_2}^{(2)}, g_{\mathbb{P}\mathbb{P}f_2}^{(5)}) = (4.0, -16.0)$  as parameter sets. The absorption effects are included here.

In Fig. 4, we show the two-dimensional distributions in  $(\phi_{\pi^+, \text{CS}}, \cos\theta_{\pi^+, \text{CS}})$  for  $\sqrt{s} = 13$  TeV and  $|\eta_\pi| < 2.5$ . We can observe interesting structures for the  $pp \rightarrow pp\pi^+\pi^-$  reaction. We show results for the individual  $\mathbb{P}\mathbb{P}f_2(1270)$  coupling terms and for the continuum  $\pi^+\pi^-$  production. Different tensorial couplings generate very different patterns which should be checked experimentally.

Some preliminary low-energy COMPASS results [22,23] suggest the presence of two maxima in the  $\phi_{\pi^+, \text{GJ}}$  distribution. So far, there are no official analogous data for high-energy scattering from either STAR or the LHC experiments. Nevertheless, we have asked ourselves the question if and how we can get a similar structure (two maxima at  $\phi_{\pi^+, \text{GJ}} = \pi/2, 3/2\pi$ ) in terms of our  $\mathbb{P}\mathbb{P}f_2$  couplings [Eqs. (2.8) to (2.14)].

In Fig. 5, we show the azimuthal angle distributions using the CS [Eq. (2.16)] and the GJ [Eq. (2.18)] frames. Here we examine the combination of two  $\mathbb{P}\mathbb{P}f_2$  couplings:  $j = 2$  [Eq. (2.9)] and  $j = 5$  [Eq. (2.12)]. We show results for the individual  $j = 2, 5$  coupling terms and for their

coherent sum. For this purpose, we fix the  $j = 2$  coupling constant to  $g_{\mathbb{P}\mathbb{P}f_2}^{(2)} = 1.0$  and assume various values for  $g_{\mathbb{P}\mathbb{P}f_2}^{(5)}$ . In the top and bottom panels, the red and green lines correspond to the results when the two couplings have opposite signs and the same signs, respectively. Different interference patterns can be seen there depending on the ratio of the two couplings,  $R = g_{\mathbb{P}\mathbb{P}f_2}^{(2)}/g_{\mathbb{P}\mathbb{P}f_2}^{(5)}$ .

Now we discuss whether the absorption effects (the  $pp$ -rescattering corrections) may change the angular distributions discussed so far in the Born approximation. We have checked that a slightly different size of absorption effects may occur for the  $j = 1, \dots, 7$  resonant terms. The absorption effects lead to a significant reduction of the cross section. However, the shapes of the polar and azimuthal angle distributions are practically not changed. This indicates that the absorption effects should not disturb the determination of the type of the  $\mathbb{P}\mathbb{P}f_2(1270)$  coupling. However, the continuum and the resonant terms may be differently affected by absorption. This will have to be

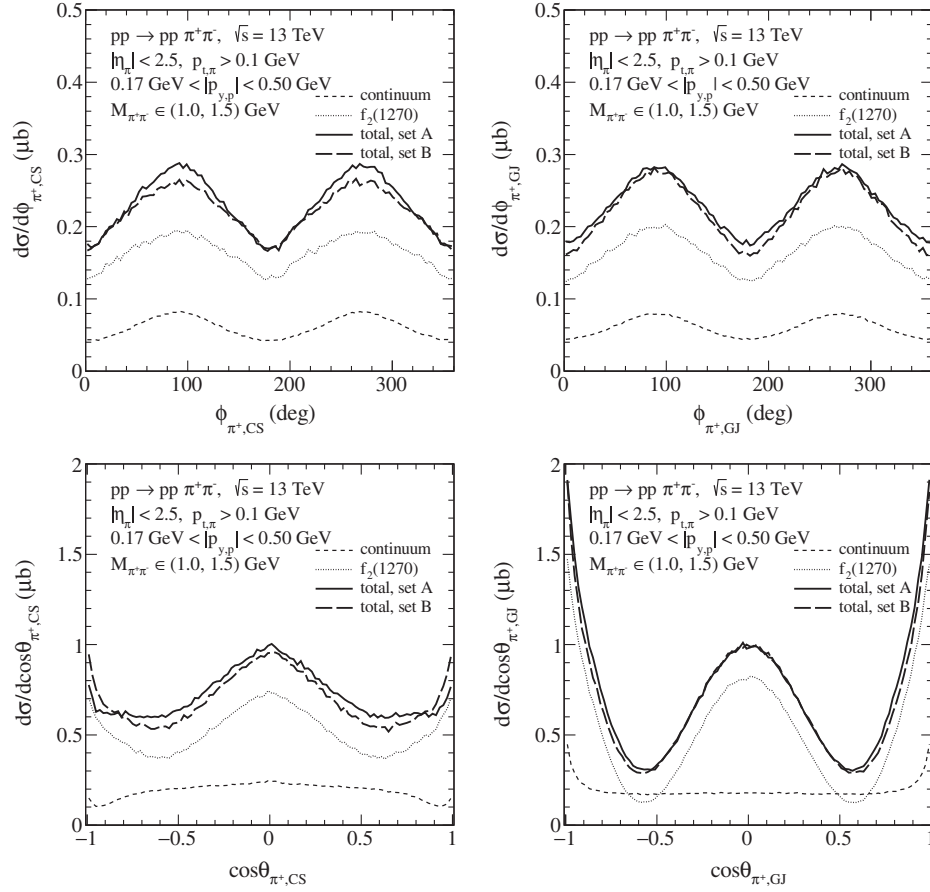


FIG. 10. The same as in Fig. 9, but for the ATLAS-ALFA kinematics:  $\sqrt{s} = 13$  TeV,  $|\eta_\pi| < 2.5$ ,  $p_{t,\pi} > 0.1$  GeV, and  $0.17 \text{ GeV} < |p_{y,p}| < 0.50$  GeV. The calculations were done in the dipion invariant mass region  $M_{\pi^+\pi^-} \in (1.0, 1.5)$  GeV. The absorption effects are included here.

taken into account when one tries to extract the strengths of the couplings from such distributions.

The measurement of forward protons would be useful to better understand absorption effects. The GenEx Monte Carlo generator [40,41] could be used in this context. We refer the reader to Ref. [42], where a first calculation of four-pion continuum production in the  $pp \rightarrow pp\pi^+\pi^-\pi^+\pi^-$  reaction with the help of the GenEx code was performed.

Clearly, by a comparison of our model results to high-energy experimental data we shall be able to determine or at least set limits on the parameters of the  $\mathbb{P}\mathbb{P}f_2(1270)$  coupling. At the moment, however, this is not yet possible, since only some, mostly preliminary, experimental distributions were presented [25–29].

In Fig. 6, we show the dipion invariant mass distributions for different experimental conditions specified in the legend. One can see the recent high-energy data from the STAR, CDF, and CMS experiments, as well as predictions of our model. Figures 6(a) and 6(b) show the preliminary STAR data from Refs. [25] and [28], respectively. Figures 6(c) and 6(d) show the CDF experimental data from Ref. [26]. Figure 6(e) shows a very recent result obtained by the CMS

Collaboration [29]. In the calculations, we include both the nonresonant continuum and  $f_2(1270)$  terms. Figures 6(b) and 6(f) show the results including extra cuts on the outgoing protons. For the STAR experiment, we take the cuts in Eq. (3.1), and for the ATLAS-ALFA experiment, we take  $0.17 \text{ GeV} < |p_{y,p}| < 0.50$  GeV. The absorption effects (the  $pp$ -rescattering corrections only) were taken into account at the amplitude level. The two-pion continuum was fixed by using the monopole form of the off-shell pion form factor with the cutoff parameter  $\Lambda_{\text{off},M} = 0.8$  GeV; see Eq. (3.18) of Ref. [7]. For the  $f_2(1270)$  contribution, in order to get distinct maxima at  $\phi_{\pi^+,GJ} = \pi/2, 3/2\pi$ , we take a combination of two  $\mathbb{P}\mathbb{P}f_2$  couplings,  $(g_{\mathbb{P}\mathbb{P}f_2}^{(2)}, g_{\mathbb{P}\mathbb{P}f_2}^{(5)}) = (-4.0, 16.0)$  (set A) and  $(4.0, -16.0)$  (set B), which correspond to the solid and long-dashed lines, respectively. The complete results indicate an interference effect of the continuum and the  $f_2(1270)$  term. For comparison, we show also the contributions of the individual terms separately.

We can see from Fig. 6 that in the  $f_2$  mass region we describe fairly well the preliminary STAR and CMS data, but we overestimate the CDF data [26]. In the CMS and

CDF measurements, there are possible contributions of proton dissociation. The continuum contribution underestimates the data in the region  $M_{\pi^+\pi^-} < 1$  GeV; however, there are also other possible processes, e.g., from  $f_0(500)$ ,  $f_0(980)$ , and  $\rho^0$  production not included in the present analysis; see, e.g., Refs. [6,7]. Also, other effects, such as the rescattering corrections discussed in Refs. [31–33], can be very important there.

We emphasize that in our calculation of the  $\pi^+\pi^-$  continuum term we include not only the leading Pomeron exchanges ( $\mathbb{P}\mathbb{P} \rightarrow \pi^+\pi^-$ ) but also the  $\mathbb{P}f_{2\mathbb{R}}$ ,  $f_{2\mathbb{R}}\mathbb{P}$ , and  $f_{2\mathbb{R}}f_{2\mathbb{R}}$  exchanges. There is interference between the corresponding amplitudes. Their role is very important, especially at low energies (COMPASS, WA102, ISR), but even for the STAR kinematics their contribution is not negligible. Adding the  $f_{2\mathbb{R}}$  Reggeon exchanges increases the cross section by 56% and 45% for the kinematical conditions shown in Figs. 6(a) and 6(b), respectively. A similar role of secondary Reggeons can be expected for the production of resonances. This means that our results for the  $f_2(1270)$  resonance (roughly matched to the STAR data) should be treated rather as an upper estimate. This may be the reason why our result for  $f_2(1270)$  is well above the CDF data.

We summarize this part by the general observation that it is very difficult to describe all available data with the same set of parameters. High-energy central exclusive data expected from CMS-TOTEM and ATLAS-ALFA will allow a better understanding of the diffractive production mechanisms.

In Figs. 7 and 8, we show the two-dimensional angular distributions for the STAR and ATLAS-ALFA kinematics, respectively. In the left panels the results for the CS system, and in the right panels those for the GJ system are presented. In the top panels we show results for the continuum term, in the center panels those for the  $f_2(1270)$  term, and in the bottom panels the results for their coherent sum. Here we take the set A with the  $\mathbb{P}\mathbb{P}f_2$  coupling parameters  $(g_{\mathbb{P}\mathbb{P}f_2}^{(2)}, g_{\mathbb{P}\mathbb{P}f_2}^{(5)}) = (-4.0, 16.0)$ . Figures 9 and 10 show that the complete results indicate an interference effect of the continuum and the  $f_2(1270)$  term calculated for the sets A and B; see the solid and long-dashed lines, respectively. The interference effect depends crucially on the choice of the  $\mathbb{P}\mathbb{P}f_2(1270)$  coupling. A combined analysis of the  $M_{\pi^+\pi^-}$  and angular distributions in the  $\pi^+\pi^-$  rest frames would, therefore, help to pin down the underlying reaction mechanism.

#### IV. CONCLUSIONS

In the present work, we have considered the possibility to extract the  $\mathbb{P}\mathbb{P}f_2(1270)$  couplings from the analysis of pion angular distributions in the  $\pi^+\pi^-$  rest system, using the Collins-Soper (CS) and the Gottfried-Jackson (GJ) frames. We have considered the tensor-Pomeron model, for which there are seven possible  $\mathbb{P}\mathbb{P}f_2(1270)$  couplings; see Eqs. (2.8)–(2.14) and Appendix A of Ref. [7]. We have shown that the shape of such distributions strongly depends on the functional form of the  $\mathbb{P}\mathbb{P}f_2(1270)$  coupling.

In particular, we have shown that the azimuthal angle distributions may have different numbers of oscillations. The corresponding distributions can be approximately represented by the formula (3.2):  $A \pm B \cos(n\phi_{\pi^+, \text{CS}})$ , where  $n = 2, 4$ . Two-dimensional distributions in the CS system  $(\phi_{\pi^+, \text{CS}}, \cos\theta_{\pi^+, \text{CS}})$ ,  $(M_{\pi^+\pi^-}, \phi_{\pi^+, \text{CS}})$ ,  $(M_{\pi^+\pi^-}, \cos\theta_{\pi^+, \text{CS}})$ , and respectively in the GJ system, will give even more information and could also be useful in understanding the role of experimental cuts. Can such distributions be used to fix the  $\mathbb{P}\mathbb{P}f_2(1270)$  coupling? The answer will require dedicated experimental studies by the STAR, ALICE, ATLAS-ALFA, CMS-TOTEM, and LHCb Collaborations. This requires comparisons of our model results with precise “exclusive” experimental data simultaneously in several differential observables.

We have shown how to select linear combinations of the different  $\mathbb{P}\mathbb{P}f_2(1270)$  coupling constants to get two maxima in  $\phi_{\pi^+, \text{GJ}}$  (or  $\phi_{\pi^+, \text{CS}}$ ) as observed at low energies by the COMPASS Collaboration; see Refs. [22,23].

In the diffractive process considered, the  $f_2(1270)$  resonance cannot be completely isolated from the continuum background, as the corresponding amplitudes strongly interfere [7]. We have discussed how the interference of the resonance and the continuum background may change the angular distributions  $d\sigma/d\cos\theta_{\pi^+, \text{CS}}$  and  $d\sigma/d\phi_{\pi^+, \text{CS}}$ . The absorption effects change the overall normalization of such distributions but leave the shape essentially unchanged. This is in contrast to the  $d\sigma/d\phi_{pp}$  distributions, where absorption effects considerably modify the corresponding shapes; see, e.g., Refs. [10,31].

In the present analysis, we have concentrated on the pronounced  $f_2(1270)$  resonance, clearly seen in the  $\pi^+\pi^-$  channel. We have discussed methods for how to pin down the Pomeron-Pomeron- $f_2(1270)$  coupling. The analysis presented may be extended also to other resonances seen in different final-state channels. We strongly encourage experimental groups to start such analyses. We think that this will bring in a new tool for analyzing exclusive diffractive processes and will provide new inspirations in searching for more exotic states such as glueballs, for instance. The exclusive diffractive processes were always claimed to be a good area to learn about the physics of glueballs. The extension of our methods to the production of glueballs, to be identified in suitable decay channels, should shed light on the Pomeron-Pomeron-glueball couplings. These represent very interesting quantities: the coupling of three (mainly) gluonic objects.

#### ACKNOWLEDGMENTS

We are indebted to Leszek Adamczyk and Rafał Sikora for useful discussions. This work was partially supported by Polish National Science Centre Grant No. 2018/31/B/ST2/03537 and by the Center for Innovation and Transfer of Natural Sciences and Engineering Knowledge in Rzeszów (Poland).

**APPENDIX: REMARKS ON THE  
TRANSFORMATION FROM THE CENTER-OF-  
MASS SYSTEM TO THE  $\pi\pi$  REST SYSTEM**

In this Appendix, we discuss the relation between quantities in the c.m. system and the  $\pi\pi$  rest system. Momenta in the c.m. system will be denoted by  $p_{\text{c.m.}}$ ,  $k_{\text{c.m.}}$ , etc.; momenta in the  $\pi\pi$  rest system by  $p_{\text{R}}$ ,  $k_{\text{R}}$ , etc. We assume that the transformation from the c.m. to the  $\pi\pi$  rest system is made by a boost—that is, by a rotation-free Lorentz transformation:

$$\begin{aligned}\Lambda(-\mathbf{p}_{34,\text{c.m.}}) &= (\Lambda^\mu_\nu(-\mathbf{p}_{34,\text{c.m.}})) \\ &= \begin{pmatrix} \frac{p_{34,\text{c.m.}}^0}{M_{\pi\pi}} & \frac{-p_{34,\text{c.m.}}^j}{M_{\pi\pi}} \\ \frac{-p_{34,\text{c.m.}}^i}{M_{\pi\pi}} & \delta^{ij} + \left(\frac{p_{34,\text{c.m.}}^0}{M_{\pi\pi}} - 1\right) \frac{p_{34,\text{c.m.}}^i p_{34,\text{c.m.}}^j}{(\mathbf{p}_{34,\text{c.m.}})^2} \end{pmatrix},\end{aligned}\quad (\text{A1})$$

where  $i, j \in \{1, 2, 3\}$ .

$$q_{1,\text{R}} = \Lambda(-\mathbf{p}_{34,\text{c.m.}})q_{1,\text{c.m.}} = \begin{pmatrix} \frac{(p_{34} \cdot q_1)}{M_{\pi\pi}} \\ \mathbf{q}_{1,\text{c.m.}} + \frac{\mathbf{p}_{34,\text{c.m.}}}{M_{\pi\pi}} \left( -q_{1,\text{c.m.}}^0 + (p_{34,\text{c.m.}}^0 - M_{\pi\pi}) \frac{(\mathbf{p}_{34,\text{c.m.}} \cdot \mathbf{q}_{1,\text{c.m.}})}{(\mathbf{p}_{34,\text{c.m.}})^2} \right) \end{pmatrix}.\quad (\text{A6})$$

With these relations, we can now express the unit vectors of the Gottfried-Jackson (GJ) system of Eq. (2.18) entirely by vectors defined in the  $\pi\pi$  rest system. We have  $p_{34} = q_1 + q_2$ , and therefore from Eqs. (A5) and (A6),

$$\begin{aligned}\mathbf{q}_{1,\text{c.m.}} \times \mathbf{q}_{2,\text{c.m.}} &= \mathbf{q}_{1,\text{c.m.}} \times \mathbf{p}_{34,\text{c.m.}} \\ &= -\frac{M_{\pi\pi}}{\sqrt{s}} \mathbf{q}_{1,\text{R}} \times (\mathbf{p}_a + \mathbf{p}_b)_{\text{R}};\end{aligned}\quad (\text{A7})$$

We have then for any four-vector  $l = (l^\mu)$

$$\Lambda(-\mathbf{p}_{34,\text{c.m.}})l_{\text{c.m.}} = l_{\text{R}}.\quad (\text{A2})$$

The reverse transformation is  $\Lambda^{-1}(-\mathbf{p}_{34,\text{c.m.}}) = \Lambda(\mathbf{p}_{34,\text{c.m.}})$

$$\Lambda^{-1}(-\mathbf{p}_{34,\text{c.m.}})l_{\text{R}} = \Lambda(\mathbf{p}_{34,\text{c.m.}})l_{\text{R}} = l_{\text{c.m.}}.\quad (\text{A3})$$

In particular, we get

$$\Lambda(-\mathbf{p}_{34,\text{c.m.}})p_{34,\text{c.m.}} = p_{34,\text{R}} = \begin{pmatrix} M_{\pi\pi} \\ 0 \end{pmatrix},\quad (\text{A4})$$

$$\begin{aligned}\Lambda(-\mathbf{p}_{34,\text{c.m.}}) \frac{M_{\pi\pi}}{\sqrt{s}} (p_a + p_b)_{\text{c.m.}} &= \frac{M_{\pi\pi}}{\sqrt{s}} (p_a + p_b)_{\text{R}} \\ &= \begin{pmatrix} p_{34,\text{c.m.}}^0 \\ -\mathbf{p}_{34,\text{c.m.}} \end{pmatrix},\end{aligned}\quad (\text{A5})$$

$$\begin{aligned}\mathbf{e}_{3,\text{GJ}} &= \frac{\mathbf{q}_{1,\text{R}}}{|\mathbf{q}_{1,\text{R}}|}, \\ \mathbf{e}_{2,\text{GJ}} &= -\frac{\mathbf{q}_{1,\text{R}} \times (\mathbf{p}_a + \mathbf{p}_b)_{\text{R}}}{|\mathbf{q}_{1,\text{R}} \times (\mathbf{p}_a + \mathbf{p}_b)_{\text{R}}|}, \\ \mathbf{e}_{1,\text{GJ}} &= \mathbf{e}_{2,\text{GJ}} \times \mathbf{e}_{3,\text{GJ}}.\end{aligned}\quad (\text{A8})$$

Note that for setting up this GJ system, only the momentum of one of the outgoing protons in the reaction [Eq. (2.1)] has to be measured—plus, of course, the momenta of  $\pi^+$  and  $\pi^-$  giving  $p_{34}$ .

- [1] C. Ewerz, M. Maniatis, and O. Nachtmann, A model for soft high-energy scattering: Tensor Pomeron and vector Odderon, *Ann. Phys. (Amsterdam)* **342**, 31 (2014).  
[2] L. Adamczyk *et al.* (STAR Collaboration), Single spin asymmetry  $A_N$  in polarized proton-proton elastic scattering at  $\sqrt{s} = 200$  GeV, *Phys. Lett. B* **719**, 62 (2013).  
[3] C. Ewerz, P. Lebedowicz, O. Nachtmann, and A. Szczurek, Helicity in proton-proton elastic scattering and the spin structure of the Pomeron, *Phys. Lett. B* **763**, 382 (2016).

- [4] D. Britzger, C. Ewerz, S. Glazov, O. Nachtmann, and S. Schmitt, The tensor Pomeron and low- $x$  deep inelastic scattering, *Phys. Rev. D* **100**, 114007 (2019).  
[5] P. Lebedowicz, O. Nachtmann, and A. Szczurek, Exclusive central diffractive production of scalar and pseudoscalar mesons; tensorial vs. vectorial Pomeron, *Ann. Phys. (Amsterdam)* **344**, 301 (2014).  
[6] P. Lebedowicz, O. Nachtmann, and A. Szczurek,  $\rho^0$  and Drell-Söding contributions to central exclusive production

- of  $\pi^+\pi^-$  pairs in proton-proton collisions at high energies, *Phys. Rev. D* **91**, 074023 (2015).
- [7] P. Lebedowicz, O. Nachtmann, and A. Szczurek, Central exclusive diffractive production of the  $\pi^+\pi^-$  continuum, scalar, and tensor resonances in  $pp$  and  $p\bar{p}$  scattering within the tensor Pomeron approach, *Phys. Rev. D* **93**, 054015 (2016).
- [8] P. Lebedowicz, O. Nachtmann, and A. Szczurek, Central production of  $\rho^0$  in  $pp$  collisions with single proton diffractive dissociation at the LHC, *Phys. Rev. D* **95**, 034036 (2017).
- [9] P. Lebedowicz, O. Nachtmann, and A. Szczurek, Towards a complete study of central exclusive production of  $K^+K^-$  pairs in proton-proton collisions within the tensor Pomeron approach, *Phys. Rev. D* **98**, 014001 (2018).
- [10] P. Lebedowicz, O. Nachtmann, and A. Szczurek, Exclusive diffractive production of  $\pi^+\pi^-\pi^+\pi^-$  via the intermediate  $\sigma\sigma$  and  $\rho\rho$  states in proton-proton collisions within tensor Pomeron approach, *Phys. Rev. D* **94**, 034017 (2016).
- [11] P. Lebedowicz, O. Nachtmann, and A. Szczurek, Central exclusive diffractive production of  $p\bar{p}$  pairs in proton-proton collisions at high energies, *Phys. Rev. D* **97**, 094027 (2018).
- [12] P. Lebedowicz, O. Nachtmann, and A. Szczurek, Central exclusive diffractive production of  $K^+K^-K^+K^-$  via the intermediate  $\phi\phi$  state in proton-proton collisions, *Phys. Rev. D* **99**, 094034 (2019).
- [13] P. Lebedowicz, O. Nachtmann, and A. Szczurek, Searching for the Odderon in  $pp \rightarrow ppK^+K^-$  and  $pp \rightarrow pp\mu^+\mu^-$  reactions in the  $\phi(1020)$  resonance region at the LHC, [arXiv:1911.01909](https://arxiv.org/abs/1911.01909).
- [14] D. Barberis *et al.* (WA102 Collaboration), A study of pseudoscalar states produced centrally in  $pp$  interactions at 450 GeV/c, *Phys. Lett. B* **427**, 398 (1998).
- [15] D. Barberis *et al.* (WA102 Collaboration), A coupled channel analysis of the centrally produced  $K^+K^-$  and  $\pi^+\pi^-$  final states in  $pp$  interactions at 450 GeV/c, *Phys. Lett. B* **462**, 462 (1999).
- [16] D. Barberis *et al.* (WA102 Collaboration), Experimental evidence for a vector-like behavior of Pomeron exchange, *Phys. Lett. B* **467**, 165 (1999).
- [17] A. Kirk, Resonance production in central  $pp$  collisions at the CERN Omega Spectrometer, *Phys. Lett. B* **489**, 29 (2000).
- [18] D. Barberis *et al.* (WA102 Collaboration), A kinematical selection of glueball candidates in central production, *Phys. Lett. B* **397**, 339 (1997).
- [19] D. Barberis *et al.* (WA102 Collaboration), A study of the  $f_0(1370)$ ,  $f_0(1500)$ ,  $f_0(2000)$  and  $f_2(1950)$  observed in the centrally produced  $4\pi$  final states, *Phys. Lett. B* **474**, 423 (2000).
- [20] F. E. Close and A. Kirk, Glueball- $q\bar{q}$  filter in central hadron production, *Phys. Lett. B* **397**, 333 (1997).
- [21] A. Breakstone *et al.* (ABCDHW Collaboration), The reaction Pomeron-Pomeron  $\rightarrow \pi^+\pi^-$  and an unusual production mechanism for the  $f_2(1270)$ , *Z. Phys. C* **48** (1990) 569.
- [22] A. Austregesilo *et al.* (COMPASS Collaboration), A partial-wave analysis of centrally produced two-pseudoscalar final states in  $pp$  reactions at COMPASS, *Proc. Sci., Bormio2013* (2013) 014.
- [23] A. Austregesilo, Central production of two-pseudoscalar meson systems at the COMPASS Experiment at CERN, Munich, Technical University Report No. CERN-THESIS-2014-190, <http://mediatum.ub.tum.de?id=1226222>.
- [24] A. Austregesilo *et al.* (COMPASS Collaboration), Light scalar mesons in central production at COMPASS, *AIP Conf. Proc.* **1735**, 030012 (2016).
- [25] L. Adamczyk, W. Guryn, and J. Turnau, Central exclusive production at RHIC, *Int. J. Mod. Phys. A* **29**, 1446010 (2014).
- [26] T. A. Aaltonen *et al.* (CDF Collaboration), Measurement of central exclusive  $\pi^+\pi^-$  production in  $p\bar{p}$  collisions at  $\sqrt{s} = 0.9$  and 1.96 TeV at CDF, *Phys. Rev. D* **91**, 091101 (2015).
- [27] V. Khachatryan *et al.* (CMS Collaboration), Exclusive and semi-exclusive  $\pi^+\pi^-$  production in proton-proton collisions at  $\sqrt{s} = 7$  TeV, Report Nos. CMS-FSQ-12-004, CERN-EP-2016-261, [arXiv:1706.08310](https://arxiv.org/abs/1706.08310).
- [28] R. Sikora *et al.* (STAR Collaboration), Recent results on central exclusive production with the STAR detector at RHIC, *Acta Phys. Pol. B Proc. Suppl.* **12**, 811 (2019).
- [29] CMS Collaboration, Measurement of total and differential cross sections of central exclusive  $\pi^+\pi^-$  production in proton-proton collisions at 5.02 and 13 TeV, Report No. CMS-PAS-FSQ-16-006.
- [30] R. Schicker *et al.* (ALICE Collaboration), Central exclusive meson production in proton-proton collisions in ALICE at the LHC, [arXiv:1912.00611](https://arxiv.org/abs/1912.00611).
- [31] P. Lebedowicz and A. Szczurek, Revised model of absorption corrections for the  $pp \rightarrow pp\pi^+\pi^-$  process, *Phys. Rev. D* **92**, 054001 (2015).
- [32] R. A. Ryutin, Central exclusive diffractive production of two-pion continuum at hadron colliders, *Eur. Phys. J. C* **79**, 981 (2019).
- [33] P. Lebedowicz, R. Pasechnik, and A. Szczurek, Measurement of exclusive production of scalar  $\chi_{c0}$  meson in proton-(anti)proton collisions via  $\chi_{c0} \rightarrow \pi^+\pi^-$  decay, *Phys. Lett. B* **701**, 434 (2011).
- [34] L. A. Harland-Lang, V. A. Khoze, and M. G. Ryskin, Modelling exclusive meson pair production at hadron colliders, *Eur. Phys. J. C* **74**, 2848 (2014).
- [35] A. Bolz, C. Ewerz, M. Maniatis, O. Nachtmann, M. Sauter, and A. Schöning, Photoproduction of  $\pi^+\pi^-$  pairs in a model with tensor-Pomeron and vector-Odderon exchange, *J. High Energy Phys.* **01** (2015) 151.
- [36] J. C. Collins and D. E. Soper, Angular distribution of dileptons in high-energy hadron collisions, *Phys. Rev. D* **16**, 2219 (1977).
- [37] D. E. Soper, Angular distribution of two observed hadrons in electron-positron annihilation, *Z. Phys. C* **17**, 367 (1983).
- [38] K. Gottfried and J. D. Jackson, On the connection between production mechanism and decay of resonances at high energies, *Nuovo Cimento* **33**, 309 (1964).
- [39] M. Goncerz, B. Rachwał, and T. Szumlak (LHCb Collaboration), Central exclusive production measurements in the LHCb, *Acta Phys. Pol. B* **49**, 1135 (2018).
- [40] R. A. Kycia, J. Chwastowski, R. Staszewski, and J. Turnau, GENEX: A simple generator structure for exclusive processes in high energy collisions, *Commun. Comput. Phys.* **24**, 860 (2018).

- [41] R. A. Kycia, J. Turnau, J. J. Chwastowski, R. Staszewski, and M. Trzebiński, The adaptive Monte Carlo toolbox for phase space integration and generation, *Commun. Comput. Phys.* **25**, 1547 (2019).
- [42] R. Kycia, P. Lebedowicz, A. Szczurek, and J. Turnau, Triple Regge exchange mechanisms of four-pion continuum production in the  $pp \rightarrow pp\pi^+\pi^-\pi^+\pi^-$  reaction, *Phys. Rev. D* **95**, 094020 (2017).